Journal of Magnetic Resonance Open 16–17 (2023) 100119

Contents lists available at ScienceDirect

Journal of Magnetic Resonance Open

journal homepage: www.sciencedirect.com/journal/journal-of-magnetic-resonance-open

Solid state nuclear magnetic resonance of polymers

Gustavo Alberto Monti [a,b,*], Rodolfo Héctor Acosta [a,b], Ana Karina Chattah [a,b], Yamila Garro Linck [a,b]

[a] Facultad de Matemática, Astronomía, Física y Computación, Universidad Nacional de Córdoba, Córdoba, Argentina
[b] Instituto de Física Enrique Gaviola, CONICET, Córdoba, Argentina

ARTICLE INFO

Keywords:
Elastomers
Entanglements
Polyelectrolytes
Relaxation
Characterization

ABSTRACT

The development of Solid-State Nuclear Magnetic Resonance (SSNMR) in Argentina took a great buster at the beginning of the 1990s along with the acquisition of many "state-of-the-art" high-field NMR spectrometers, two of them multipurpose solid-liquid spectrometers. From then to nowadays, the study of solid samples, including polymers, has been a current topic at the NMR group of the Facultad de Matemática, Astronomía, Física y Computación of Universidad Nacional de Córdoba, in Argentina. In this work, we propose a review approach of several research works on solid polymers performed in our group, covering low-field relaxation studies and high-resolution SSNMR.

1. Introduction

Polymers have been present in daily life for thousands of years. Natural fibres for dressing and cellulose for paper are the most ancient uses of natural polymers. At the beginning of the 1900s research [1] showed that polymers are structured in repetitive "identical" units named monomers, linked to each other by covalent bonds. The development of synthesis techniques and molecular analysis allowed for the control of polymer structure and opened a myriad of different applications for polymer materials. This work aims to present a review of applications of SSNMR to study different polymer systems, carried out at the NMR group in Córdoba, Argentina from the year 2000 to nowadays.

From a general point of view, NMR may be divided into time-domain (TD) and spectroscopic experiments, where a combination of both is often desirable. TD-NMR in polymers relies on the influence of signals due to the modulation of dipolar interactions driven by molecular motions, particularly the buildup of multiple quantum coherences (MQC) [2–6] in the decay of transverse magnetization [7–9]. On the other hand, the orientation dependence of interactions in solids drives the unique features of polymer spectra [10]. Naturally, a combination of both techniques, where a TD block tags the spectra acquired in a second dimension is a powerful tool for polymer characterization [11].

A set of polydimethylsiloxane (PDMS) model networks, carefully synthesized with a controlled number of defects and functionalities, was used to exemplify how MQC information may be directly correlated with the system elastic response. Further, we showed that not only the discrimination of chemical and physical crosslinks was possible and that the timescales on which they occur may be derived from transverse relaxation experiments [12,13].

Different techniques involving high-resolution spectroscopy in dilute nuclei (^{13}C, ^{15}N) offer invaluable information on new materials related to polymeric systems, particularly poly(ethylenimine) polymers and hydrogel networks. Linear poly(ethylenimine) (PEI) has many applications, for example, as a cosmetic ingredient to adjust viscosity, as a chelating metal ion to inhibit corrosion, and as a copolymer to develop energy storage devices, among others. Cooper complexes of hydrogels have attracted attention for industrial applications such as the removal of toxic heavy metal ions from aqueous media and the recovery of gold from HCl solutions. Because of the importance of mentioned materials, their characterization in the solid state has attracted attention in recent years, and from the NMR point of view. This is particularly useful when the polymeric systems have a degree of amorphous character, that is possible not only to characterize but also to quantify. Finally, 1D and 2D solid-state NMR spectroscopy techniques were applied to characterize the homogenous character of three variants of linear PEI systems with different molecular weights, and the cooper ion uptake from different hydrogels with polyampholyte and polyelectrolyte behavior at different concentrations of the metal ion [14–16].

* Corresponding author.
E-mail address: gustavo.monti@unc.edu.ar (G.A. Monti).

https://doi.org/10.1016/j.jmro.2023.100119

Available online 2 May 2023

2. Theory

2.1. Polymer dynamics

Polymers are complex materials. If cooled down from the melt the system can transform into a crystalline or semicrystalline polymer below its melting temperature T_m, or a glassy polymer below its glassy temperature transition T_g [17]. A semicrystalline polymer consists of regions of crystalline chains packed parallel to each other and intercalated between them by amorphous regions. When polymer chains in a melt react with the others, a cross-linked network structure can arise. Due to the local motion of the chains, polymer networks at temperatures above their T_g e are considered "soft". Polymer networks with T_g below room temperature are named "elastomers".

The mechanical response of polymeric materials is strongly correlated to their structure. In the particular case of polymer networks, chemical or physical cross-linking points give distinctive characteristics to these materials such as high elastic elongation, good thermal stability, and insolubility. Polymer networks can be obtained by random cross-linking reactions [18] or synthesized with a well-controlled number of defects [19,20].

The dynamics of flexible polymer chains have attracted great interest for years. At equilibrium, these chains adopt a variety of conformations giving rise to many different types of movements, according to the temporal and spatial scale of observation. Generally, fast dynamics is related to the chain`s movements at a short spatial scale, while slow dynamics corresponds to movements at a long spatial scale. The chemical structure determines the fast and local motion of chemical bonds, as in low molecular weight molecules. However, at a large scale, the polymer chain exhibits dynamic properties that are not present in small molecules. These properties are almost universal for polymeric chains with different chemical structures.

The characteristic motion of the polymer chain is responsible for several dynamic properties, i.e. viscoelastic, dielectrics, and diffusive properties. The viscoelastic properties have been studied since a long time ago [21]. Viscoelasticity means that these materials respond, under the action of external forces, in a way that remembrance either elastic behavior in solids or viscous behavior in liquids.

For polymer networks, those properties are strongly correlated to the network structure: cross-link point density, a fraction of the elastic active chains, molecular weight between cross-link points, topological defects, and entanglements.

Theories attempting to model cross-linked polymers' behavior treat the networks as ideal units [22]. A condition satisfied by ideal networks is to be formed just solely by elastic active chains responding to a Gaussian statistics distribution [23,24]. However, the predictions based on those ideal networks must be revised because, as we show below, actual polymeric networks contain defects (see Fig. 2.1.1) [19,25].

The most important models to describe network polymer elasticity were introduced by Hermans, Flory, and Wall [26,27], the, "affine model", and James and Guth, the "phantom model" [28,29]. In the affine model, the relative deformation of each segment of the network is equal to the macroscopic deformation applied to the network itself. According to that, the network is formed by elastic cross-link points fixed in the space. The elastic chains are permanently attached to these cross-link points. In real networks, the crosslink points are not fixed in space. They can fluctuate around their mean positions. These fluctuations are incorporated in the "phantom model" [29], being the main difference between phantom and affine models [17].

2.2. T_2 relaxation

First, we present some theoretical details for the analysis of time-domain ^{1}H NMR T_2 relaxation, when applied to the study of the dynamics of linear guest and structural pendant chains in polymers. In the analysis of the ^{1}H NMR experiments, the transverse magnetization decay

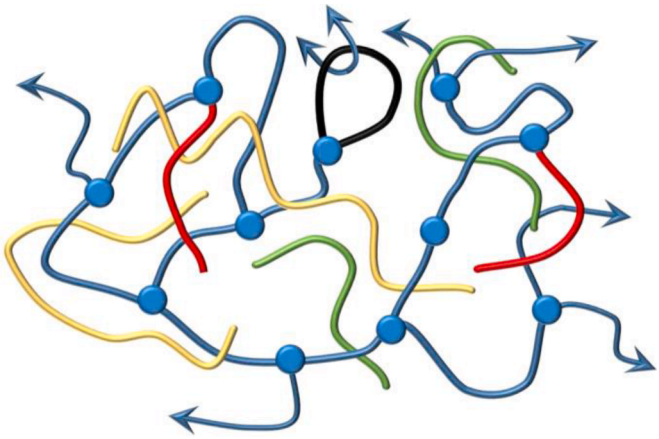

Fig. 2.1.1. Schematic representation of model PDMS networks obtained via the end-linking technique. Here the tri-functional crosslinkers are indicated with circles, elastic di-functional chains with blue lines, and linear guest chains with yellow lines. An entangled loop that contributes to the network elasticity is indicated with a black line. Green and red lines represent soluble and pendant material, respectively.

can be described as the sum of a solid-like contribution, with relative weight W_e, coming from elastically active chains and transient entanglements persisting on the NMR time scale, in addition to a liquid-like contribution, with relative weight W_p, coming from the fraction of relaxed guest and pendant material [30]. The decay of the total transverse magnetization can be described by the equation [31]:

$$M(t) = \mathrm{M}_0\{W_e exp[- t/T_2 - qM_2\tau_s^2(exp(-t/\tau_s) + t/\tau_s - 1)] + W_p exp(-t/T_2)\} \quad (2.1)$$

If our interest is mainly to quantify the mass fraction of elastic and pendant chains as observed by ^{1}H NMR, the functional form of Eq. (2.1) is an appropriate model to describe the behavior of the total magnetization $M_x(t)$ as was shown in our previous work [30].

In an NMR experiment at temperatures above T_g a polymer network is a system that contains different mobile molecular parts, which produce distinguishable relaxation signals. Namely Elastically active chains, (b) dangling or pendant chain ends, and (c) soluble molecules (see Fig. 2.1.1). For fast local motions, correlation times $\tau_f \sim 10^{-8}s$ may comprise molecular group reorientation, intra-Kuhn segments isomerization, and reorientation of the Kuhn segments by Rouse modes. Elastic chains are fixed at both ends, and this constraint induces an anisotropy in their fast motions. Consequently, a small, mean residual part $q \sim 10^{-4}s$ of the second moment of the dipolar interaction at rigid lattice remains. This residual part is further reduced by slower motions of the chain. These slower motions correspond to collective modes involving larger segments of the chain and can be characterized by a correlation time $\tau_s \sim 10^{-3}s$. The mean residual qM_2 produces the solid-like behavior of the magnetization decay of the elastic chains. Similar behavior is expected for entangled chains, within the NMR time scale. As the dangling or pendant chain ends are fixed to the network by one end, their motion is mainly isotropic. The magnetization of the soluble chains shows a behavior like that of the dangling chain ends.

The residual second moment of the dipolar coupling is $M_2^{RES} = qM_2^{RL}$, where q is the anisotropy parameter and M_2^{res} is Van Vleck's second moment of the dipolar interaction in the rigid lattice. The NMR observed parameter is the residual dipolar coupling D_{res}, and is related to the second moment as $M_2^{res} = \left(\frac{9}{20}\right)D_{res}^2$.

2.3. Polymer network defects

2.3.1. Pendant chains

The contribution of unrelaxed pendant material to the elastic response in NMR experiments can be determined as follows. Taking into account the probability distribution of the primitive path lengths at equilibrium and the tube diameter, the free end of the pendant chain can be thought of as undergoing a Brownian motion in a suitable potential field. The probability distribution for arm retraction is then the solution of the Smoluchowski equation for the probability of the deepest penetration as a function of time. The Pearson-Helfand model predicts that the potential has a quadratic form [32–35],

$$U_{PH} = \frac{15}{8} n_e s^2. \tag{2.2}$$

Here n_e is the number of entanglements per pendant chain, and s ($0 < s < 1$) is the fractional distance back along the primitive path the free end has been retracted. At long times, $t > \tau(s = 1/\sqrt{n_e})$, the slow relaxation process is controlled by the so denominated "First-Passage-Time" $\tau_s(s)$. The solution to the first passage time for this problem can be expressed as $\tau_s(s, n_e) = -\frac{15}{16}\frac{I\pi^3 n_e^3 \tau_e}{\alpha} erf(I\sqrt{\alpha\, n_e}\, s)$, where $I = \sqrt{-1}$ and erf(x) is the error function [33]. At short times, $t < \tau(s = 1/\sqrt{n_e})$, the relaxation process is dominated by a one-dimensional Rouse-like dynamic characterized by $\tau_f(s)$ [36], where

$$\tau_f(s) = \frac{225\pi^3}{256} \tau_e n_e^4 s^4. \tag{2.3}$$

Here τ_e is the Rouse time between entanglements and can be determined through independent experiments with linear chains[32]. The relaxation time $\tau(s)$ can be determined through a crossover formula considering both timescales [32,36]. Taking into account the molecular weight distribution of the pendant material, the fraction of unrelaxed material at time $t = \tau_\alpha$ can be determined as (here $\tau_\alpha \sim 1$ ms):

$$g_p = \int_0^\infty dn_e \int ds\, P(n_e)\, \exp[-\tau_\alpha / \tau(s, n_e)]. \tag{2.4}$$

Here $P(n_e)$ is the relative volume fraction of defects with an average number of entanglements n_e. $P(n_e)$ can be determined through the molecular weight distribution of pendant and elastic chains and the mean-field description of the network structure ($\int_0^\infty dn_e P(n_e) = 1$).

2.3.2. Linear guest chains

According to the classical Doi–Edwards–de Gennes tube model, the relaxational dynamics of an entangled polymer chain can be separated into different regimes depending on the length and time scales. At very short times, the segments are considered to undergo unrestricted Rouse motion where the segments move freely without any constraint other than chain connectivity. At longer times, the chain "discovers" the constraints imposed by the confining tube, and then polymer conformation relaxes through constrained-Rouse dynamics. However, although this model captures the dominant features of the entangled polymer dynamics, there are important shortcomings [37]. To remove discrepancies, Milner and McLeish's model includes a contribution from contour-length fluctuations determined by considering the entangled linear chains as two-armed stars [37]. At the millisecond time scale of NMR experiments, the Rouse modes are completely relaxed, and their contribution is negligible. The dominant contribution to the anisotropic response become the addition of a term corresponding to the loss of memory of the chain ends due to contour-length fluctuations, and another term due to the escaping the remainder of the tube, by reptation.

Within the theoretical frame of Milner and McLeish, during the retraction, the fraction of tube surviving from the initial configuration, can be expressed as [37]:

$$\Phi_{retr} = \int ds\, \exp[-t / \tau(s)] \tag{2.5}$$

At short times the fast relaxation process is dominated by a one-dimensional Rouse-like dynamic characterized by $\tau_f(s)$, Eq. 2.3. At longer times, retraction becomes increasingly slow, and most of the remaining chain segments will relax their configurational memory by reptation [37],

$$\Phi_{rept} = \Phi_{retr}(\tau = \tau_s) \sum_{p\ odd} \frac{8}{\pi^2 p^2} exp(-p^2 t / \tau_d) \tag{2.6}$$

Then, the fraction of trapped entanglements $g_g(t)$ results:

$$g_g(t) = \Phi_{retr} + \Phi_{rept} \tag{2.7}$$

while the relaxed fraction $[1 - g_g(t)]$ behaves as isotropic.

3. Experimental methods

3.1. Transverse relaxation acquisition

The T_2 values were acquired either using the very well-known Carr-Purcel-Meihboom-Gill (CPMG) pulse sequence. The CPMG is applied along the MLEV-4 pulse phase cycle, this assures that the T_2 data acquired with this pulse sequence match exactly the T_2 data acquired with the Hahn Echo pulse sequence [38].

3.2. Double quantum coherences acquisition

Proton Double Quantum (DQ) experiments were performed following the procedures developed by Saalwächter et al. [39]. The experiment relay on the excitation of multiple quantum coherences between two or more dipolar coupled spins, providing a method for measuring the homonuclear residual dipolar coupling constant, D_{res}, between spins in polymeric networks. The pulse sequence consists in an excitation period where the desired coherences are "build up". An evolution period under the action of the Hamiltonian of the system. A reconversion period that allows to convert the coherences to observable magnetization. Finally, the detection of transverse magnetization. A 4-step phase cycling selects a double quantum-filtered intensity (S_{DQ}) (for details see supplementary material). The DQ signal provides information about the structure of the polymeric chains and hence on the residual dipolar coupling constant D_{res} values and their distribution.

The residual dipolar couplings can be obtained from the intensities I_{nDQ}. Using intensities $I_{nDQ} \leq 0.45$ the data are fitted with an inverted Gaussian function based on static second-moment approximations [3]:

$$I_{nDQ} = \frac{1}{2}\left[1 - \exp\left(\frac{2}{5} D_{Res}^2 \tau^2\right)\right] \tag{3.1}$$

Here D_{res} is an apparent residual dipolar coupling that represents an average over different internuclear spin pair couplings. If a substantial distribution of dipolar couplings is present, an average residual dipolar coupling (D_G), as well as the standard deviation (σ_G), can be obtained by [40,41]

$$I_{nDQ}(D_G, \sigma_G) = \frac{1}{2}\left[1 - \frac{\exp\left(-\frac{\frac{2}{5}D_G^2\tau^2}{1+\frac{4}{5}\sigma_G^2\tau^2}\right)}{\sqrt{1+\frac{4}{5}\sigma_G^2\tau^2}}\right] \tag{3.2}$$

Fig. 3.2.1 shows a typical example of the DQ build-up curve in a polydimethylsiloxane network melt.

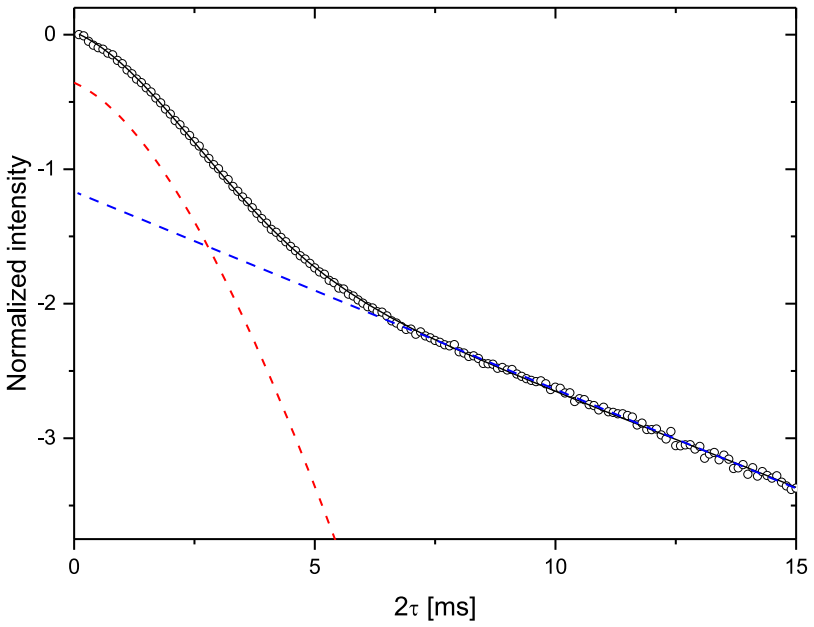

Fig. 3.1.1. Typical TD magnetization evolution of a PDMS sample under a CPMG pulse sequence. The solid-like (Gaussian decay) and the liquid-like (exponential decay) behaviours are observed.

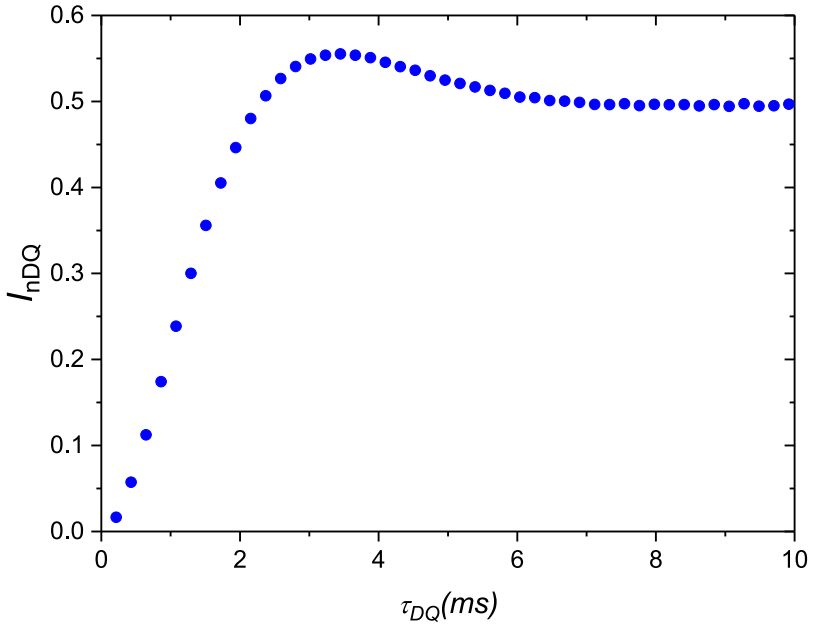

Fig. 3.2.1. DQ Build-up curve on a typical PDMS network.

4. Results and discussion

4.1. Polydimethylsiloxane model networks

In one of our first works, we studied a model polydimethylsiloxane polymer network in collaboration with colleagues of PLAPIQUI-CONICET and the Physics Department of Universidad Nacional del Sur, Bahía Blanca, Argentina. As mentioned in Section 2, polymer networks contain a complex structure characterized by the presence of elastically active chains, which are those chemically connected to the gel structure at their extremes; free chains (soluble) trapped in the network and pendant chains connected to the gel by one of their end units. Free and pendant chains are the most common type of defects. The structure and concentration of these defects affect considerably the equilibrium and dynamic properties of networks [42,43].

To study the influence of network defects on their properties, it is convenient to work with systems with controlled amounts of well-characterized defects. Our work was done on model PDMS networks, which constitute an ideal system to reveal the basic mechanisms responsible for the structural behaviors of more complex systems [19,20,30,44]. Model networks have proved to be very useful to elucidate the basic mechanism of relaxation in polymers with branched structures [33].

The notation employed to identify the different networks is *f*-$B_{2,i}$-$B_{1,j}$-XX. $B_{2,i}$ with $i = 1$–3 identifies the bifunctional end-linked PDMS that generate the elastic chains, with molecular weights of 21 500, 23 900 and 11 900 g/mol. $B_{1,j}$ categorizes the monofunctional prepolymers employed to make the pendant chains with molecular weights of 26 500,

51 300, 60 600, 83 500, and 121 300 g/mol. The last number, XX, indicates the weight fraction of the monofunctional chain employed in the formulation of each network. Finally, *f* (3 or 4), identify the cross-linking functionality.

After the extraction of solubles [20], the mass fraction of elastic (W_e) and pendant chains (W_p=1-W_e) were determined through mean-field calculations. These calculations indicate that pendant material is mainly constituted by reacted B_1 chains and partially reacted B_2 chains [20].

4.1.1 Quantification of elastic and pendant chains in polymer networks

In our first work on PDMS networks [30] we estimated the mass fraction of elastic and pendant chains using transverse proton relaxation in NMR. These experiments were compared with theoretical estimations of the mass fraction of pendant chains predicted by mean-field calculations (MFC). The observed difference was due to the fact that, at the frequencies normally used at ^{1}H NMR, only the un-entangled part of the pendant chains is detected. Under these conditions, the entangled fraction of pendant chains behaves as an elastic portion of the chains.

Single B_2 chains reacted with the gel by one of the end-functional groups belonging to the un-entangled portion of pendant chains and are counted by NMR as pendant material. By utilizing a recursive model it was possible to calculate the mass fraction of B_2 chains that both belong to the pendant material and have just one reacted end [19,44,45]. On the other hand, the entangled part of longer pendant chains also behaves as elastic chains.

The values given by the model for the two networks prepared exclusively with B_2 chains were in very good agreement with those obtained by NMR. The rest of the networks were prepared by adding monofunctional chains (B_1) to the reaction system described before. In this case, the length of monofunctional chains was changed to verify the influence of entanglements. All the monofunctional chains used had a molecular weight higher than the critical molecular weight between entanglements. For this reason, only the unentangled ends of the B_1 chains could be detected as pendant material by ^{1}H NMR relaxation experiments.

It was shown that the mass fraction of pendant chains observed by ^{1}H NMR relaxation experiments are given by the pendant bifunctional molecules with only one end reacted plus the unentangled end of the monofunctional chains. When the NMR results were compared with the theoretical calculations that take into account the presence of entanglements, a very good agreement was found as can be seen in Fig. 4.1.1 for a set of trifunctional networks.

4.1.2. Study of structural and dynamical properties of polymer networks via DQ-NMR

We have applied DQ NMR techniques to study the structural and dynamical properties of model silicone polymer networks. The systems analyzed were a set of polymer networks with small relative variations between them, of the average molecular weight of the elastically active chains, the molecular weight of pendant chains, and the concentration of pendant chains [46]. Changes induced by these defects in the residual dipolar couplings were related to changes in the viscoelastic relaxation times and compared against the behavior of the elastic shear modulus. A very good correlation between NMR measurements and the corresponding rheological experiments was found.

It can be shown that the dependence of the residual second van Vleck moment on cross-linking density is described by the following equation [47]

$$M_2 \sim 1/N^2 \tag{4.3}$$

where N is the effective number of statistical segments which, on a microscopic scale, represents the average chain length between both chemical and physical cross-links [48]. If we assume a linear dependence of elastic modulus *G* with *1/N*, as is the case of an ideal polymer network, a linear dependence of *G* with $\sqrt{M_2}$ is expected. In Fig. 4.1.2 we show $\sqrt{M_2}$ vs *G* for all the networks where a linear correlation can be observed [3].

4.1.3 Unreactive linear guest chains

We have also investigated a series of model end-linked polymer networks with varying contents of unreactive linear guest chains [49]. The time−temperature superposition (TTS) was employed to expand the characteristic time scales of NMR exploration by about 2 orders of magnitude. A comparison between swelling data and tube model predictions shows that NMR can observes the dominant characteristics of

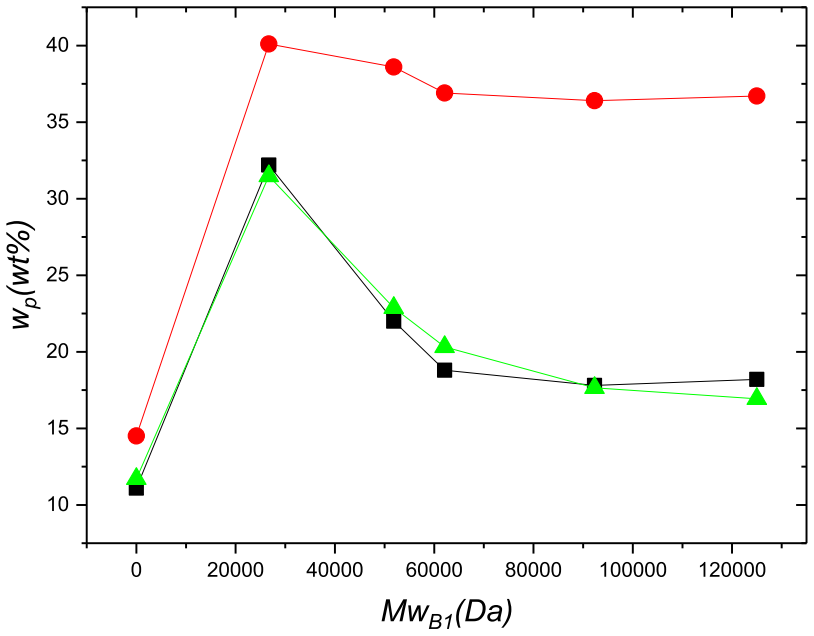

Fig. 4.1.1. Mass fraction of pendant chains (W_p) as a function of weight-average molecular weight of monofunctional chains added (Mw_{B1}). Networks prepared with a trifunctional crosslinker ($f = 3$). Symbols: (▲triangle) ^{1}H NMR values, (●) values predicted by mean-field theory (recursive approach), and (■) values calculated with eq 4.2. Adapted with permission from Ref. [30] Copyright 2001 American Chemical Society.

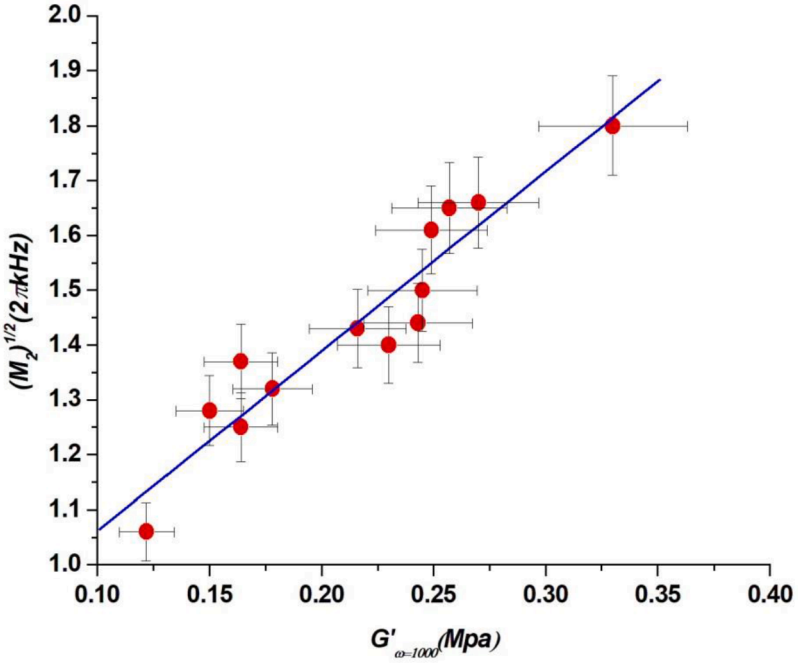

Fig. 4.1.2. $(M_2)^{1/2}$ as a function of the elastic modulus ($G_{w=1000}$) for networks $B_{2,1}$, $B_{2,2}$, $B_{2,3}$. Adapted with permission from Ref. [46] Copyright 2006 American Chemical Society.

Table 4.1.1
Molar mass characterization of unreactive guest chains.

Network	M_n(kg/mol)	M_w/M_n	*r*	$W_{BO}(g/g)$	$W_s(g/g)$	φ	$W_g^{sw}(g/g)$
3-B_2–00			0.998		0.004	0.25	
3-B_2-$B_{0,1}$–20	47.8	1.07	1.005	0.196	0.183	0.22	0.01
3-B_2-$B_{0,2}$–05	97.2	1.24	1.035	0.049	0.031	0.24	0.02
3-B_2-$B_{0,2}$–10	97.2	1.24	1.005	0.099	0.057	0.23	0.04
3-B_2-$B_{0,2}$–20	97.2	1.24	1.015	0.196	0.132	0.20	0.06

W_s: amount of soluble material extracted through swelling experiments. ϕ: degree of swelling in toluene. W_g^{sw}: fraction of guest chains that remain in the network after swelling experiments. *r* degree of reaction.

the equilibrium and dynamic properties of defects trapped in slightly cross-linked, entanglement-dominated polymer networks. The high-temperature experiments are necessary because we need to ensure complete relaxation of the guest linear chains on the millisecond time scale of the NMR experiments to obtain an accurate description of the network architecture. Contents of guest chains determined by NMR were found to agree within a 1 wt% accuracy with data of swelling experiments.

A set of model polymer networks were synthesized with different concentrations of linear (guest) soluble polymer chains. The characteristics of the networks are shown in Table 4.1.1. The system is then composed of a fully reacted $A_3 + B_2$ network (B_2: $M_w = 21\ 300$ g/mol; $M_w/M_n = 2.95$, A_3 phenyltris(dimethylsiloxy)silane cross-linker), pendant material consisting of partially reacted groups that are linked to the network by one end, and soluble material from unreacted or partially reacted precursors and B_0 guest chains (see scheme in Fig. 2.1.1).

These values, w_e and w_d, were extracted from the CPMG experiments by a nonlinear least-squares fitting procedure. In Fig. 4.1.3, the fraction of elastic material is plotted as a function of temperature.

As the time scale of NMR observation is fixed around 1 ms, the transient solid-like contribution coming from the unrelaxed fraction of pendant and guest chains is affected by temperature. Upon temperature increase, a higher fraction of the chain ends of guest and pendant material becomes isotropic. Hence, it should be expected that if the terminal relaxational time of defects becomes shorter than 1 ms, the solid-like contribution decays and eventually reach a plateau at high temperatures.

On the other hand, the fraction of elastically active chains and the permanently trapped entanglements generated by the cross-linkers cannot modify their contribution to the solid-like response with temperature because the elastic chains are linked to the network through both ends [50]. The temperature-dependent fraction of elastic material $w_e(T)$ determined by NMR can be expressed as:

$$w_e(T) = W_e(T) + g_p W_p(T) + g_g W_g(T) \tag{4.4}$$

where W_e, W_g, and W_p represent the fraction of elastic, guest, and pendant chains, respectively. Here $g_p(T)W_p$ and $g_g(T)W_g$ are the temperature-dependent fractions of unrelaxed pendant and soluble (linear guest) material, respectively. A decrease of the ~1% of the elastic

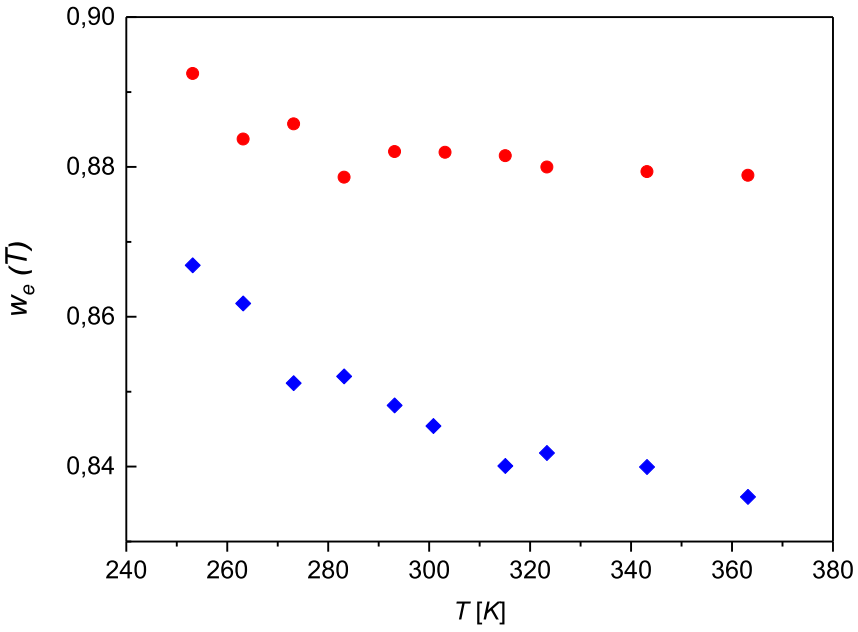

Fig. 4.1.3. Elastic fraction as a function of the temperature for samples prepared with an initial content of 5% of $B_{0,2}$ guest chains (circles) and 20% of $B_{0,2}$ guest chains (diamonds). Reprinted with permission from Ref. [49] Copyright 2016 American Chemical Society.

Table 4.1.2
Experimentally Determined Parameters for the Fraction of Guest (W_g NMR), Pendant (W_p NMR), and Elastic Chains (W_e NMR) Present in the Networks Determined by Fitting Eq (4.5) to the NMR Data.

network	$W_p^{NMR}(g/g)$	$W_e^{NMR}(g/g)$	$W_g^{NMR}(g/g)$	$W_g^{sw}(g/g)$
3-B_2–00	0.110	0.890	0.00	
3-B_2-$B_{0,1}$–20	0.110	0.886	0.004	0.01
3-B_2-$B_{0,2}$–05	0.108	0.871	0.021	0.02
3-B_2-$B_{0,2}$–10	0.107	0.861	0.032	0.04
3-B_2-$B_{0,2}$–20	0.103	0.833	0.064	0.06

fraction $w_e(T)$ was observed as the temperature increases (see Fig. 4.1.3) for the network B_2-$B_{0,2}$–05, while for the network B_2-$B_{0,2}$–20 we change from 87% to almost 84% for the same temperature range. This different behavior should be expected if we consider that networks B_2-$B_{0,2}$–05 and B_2-$B_{0,2}$–20 exhibit different fractions of guest chains (see W_g^{sw} in Table 4.1.2).

The tube model theory combined with TTS can be employed to quantify the transient contributions of guest and pendant chains to w_e(T). Since the slow dynamics of pendant and linear guest chains involve different mechanisms of relaxation, we employ the approaches described in Sections 2.3.1 and 2.3.2 to obtain g_p and g_g in Eq (4.4).

. The time−temperature superposition principle was applied to $w_e(T)$ data to obtain the fraction of elastic material as a function of time, $w_e'(t)$. The corresponding horizontal shift factor, a_T, was determined considering an activation energy $E_a \sim 29$ kJ/mol [20] and a reference temperature of $T_0 = 313$ K.

Considering that for PDMS networks D_{res} is about 250 Hz [13], and for melts with chains of M_w around 130 kg/mol and less, D_{res} is ca. 100 Hz; the motional narrowing condition is in the range $\tau = 1/2\pi D_{res} = 1.6 - 0.6$ ms. Therefore, a characteristic time of 1 ms was considered for the relaxation of the chains, see Fig. 4.1.4. It is worthwhile to mention that within the temperature regime analyzed here the time window of exploration increases by almost 2 orders or magnitude thanks to TTS ($a_T = 253/a_T = 363 \sim 70$). Eq. (4.4) is then expressed as

$$w_e'(t) = W_e + g_p(t)W_p + g_g(t)W_g \quad (4.5)$$

Here W_e and W_g were determined by fitting NMR $w_e'(t)$ data by Eq (4.5) (see Table 4.3.2). In Figure 4.3.3, NMR data for network B_2-$B_{0,2}$–20 is shown, together with the corresponding fitting to Eq. 2.7. The contribution to the elasticity of guest chains, $g_g(t)W_g$, and that of the pendant chains, $g_p(t)W_p$, are presented separately to be able to compare both contributions. The contribution of the free defects to elasticity is only relevant at short times.

In summary, we show that the slow dynamics of PDMS network defects could be directly monitored by NMR proton spin relaxation as a function of temperature. Application of the time−temperature superposition principle to NMR parameters allowed an accurate determination of the contribution of different types of defects to the relaxation processes. The temperature-dependent apparent defect contents, and their contribution to elasticity, could be described by combining tube, reptation, and arm retraction concepts. As high-temperature experiments ensure complete relaxation of the guest linear chains, accurate quantification of the content of elastic and pendant chains within the network was possible.

4.1.4. Networks with mixed functionality

We obtained further insights on the correlation between elasticity and network architecture, by performing DQ-NMR experiments [12]. We studied the relationship between D_{res} obtained by DQ experiments and topology of PDMS networks, with different average functionalities and accurately controlled contents of defects. Characteristics of the networks are shown in Table 4.1.3.

The molecular weight for the difunctional precursors was $M_n = 7900$ g/mol. The molecular weight between cross-links M_c was calculated by the recursive method [19]. The fraction of relaxed pendant chains are determined both from CPMG experiments [49] ($(1-\phi)_{TD}$) and from DQ experiments [40] ($(1-\phi)_{DQ}$), showing a good agreement.

The simplest models that capture the elastic behavior of polymer networks, in terms of the average size of the polymer chains that make up the system (network strands) and the functionality of cross-linker points, are the affine and phantom ones [27,29]. According to the phantom model, the elasticity of the network is reduced by a factor $(f-2)/f$, with f being the functionality of the cross-linker. These models can underestimate the elasticity of real networks due to the contribution of trapped entanglements [51–57].

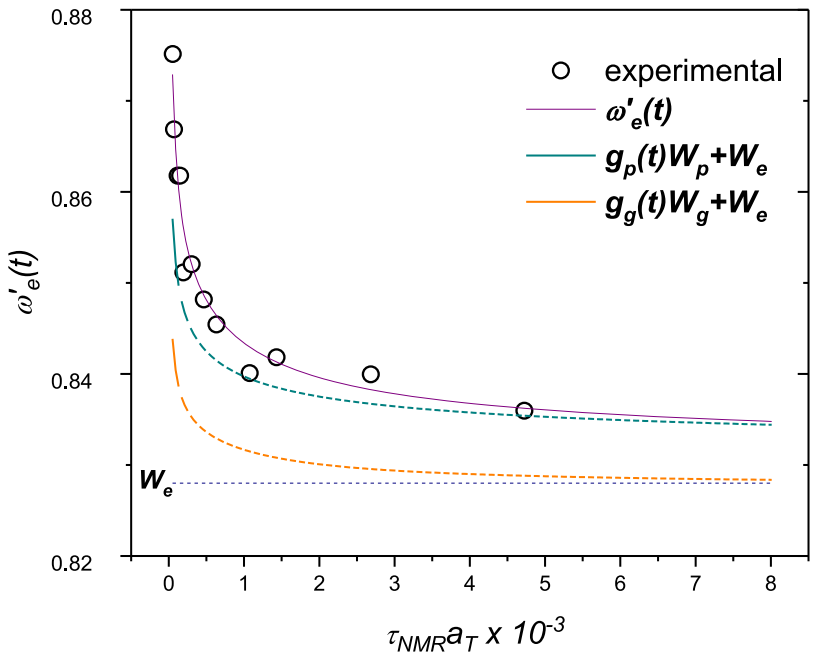

Fig. 4.1.4. Elastic fraction determined by NMR as a function of time ($w'_e(t)$) for network 3-B_2-$B_{0,2}$–20. At the time scale of NMR testing, an unrelaxed fraction of guest $g_g(t)$ and pendant $g_p(t)$ material contributes to the solid-like response. Reprinted with permission from Ref. [49] Copyright 2016 American Chemical Society.

Table 4.1.3
Networks with Variable Functionality (f), Weight Fraction of Cross-Linkers with Variable Functionality (W_{A4}; W_{A8}), and Networks with Addition of Pendant Chains with Variable Weight Fractions (W_{B1}).

network	Cross-linker	W_{A4} (wt%)	W_{A8} (wt%)	f	W_{B1} (wt%)	M_{nB1} [g/mol]	M_c [g/mol]	M_C/M_{nB2}	$D_{res}/2\pi$ [Hz]	$(1-\emptyset)_{TD}$	$(1-\emptyset)_{DQ}$
3–100-B_2–00	A_3	–	–	3	–	–	9460	1.19	202	0.07	0.07
4–25-B_2–00	$A_3 + A_4$	0.254	–	3.25	–	–	8657	1.09	220	0.06	0.06
4–60-B_2–00	$A_3 + A_4$	0.598	–	3.60	–	–	8590	1.09	243	0.05	0.05
4–75-B_2–00	$A_3 + A_4$	0.745	–	3.76	–	–	8460	1.07	251	0.04	0.04
4–100-B_2–00	A_4	1.000	–	4	–	–	8410	1.06	263	0.05	0.05
8–100-B_2–00	A_8	–	1.000	8	–	–	8160	1.03	352	0.06	0.06
8–25-B_2-B_1–001	$A_3 + A_8$	0.744	0.256	5	0.010	51,300	8120	1.03	255	0.10	0.09
8–25-B_2-B_1–005	$A_3 + A_8$	0.752	0.248	5	0.051	51,300	8540	1.08	242	0.11	0.10
8–25-B_2-B_1–010	$A_3 + A_8$	0.748	0.252	5	0.102	51,300	8520	1.08	232	0.13	0.14
8–25-B_2-B_1–015	$A_3 + A_8$	0.750	0.250	5	0.149	51,300	8700	1.10	228	0.16	0.16

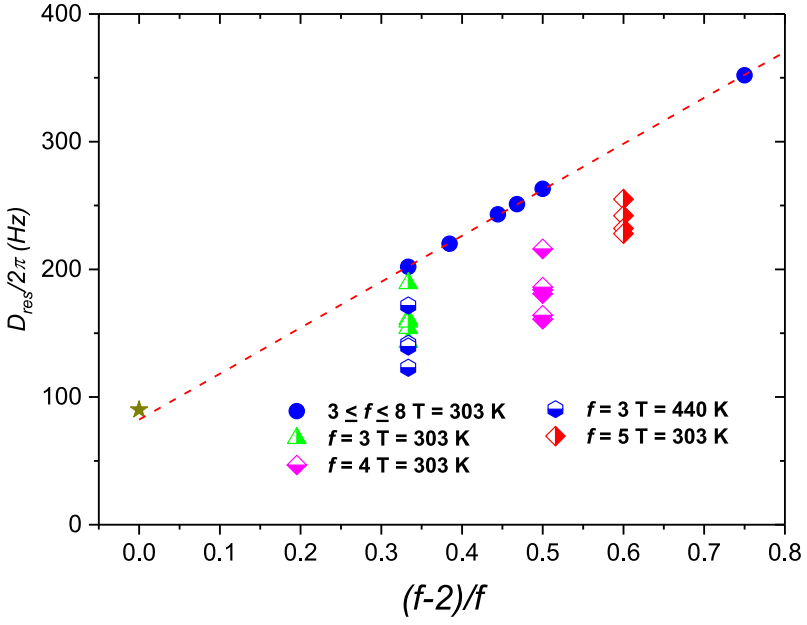

Fig. 4.1.5. Residual dipolar coupling constant determined by NMR as a function of $(f-2)/f$. Networks with varying average functionality without defects (dots) follow a linear behavior (dashed line). Networks with different concentrations of pendant chains are not well represented by the phantom model (half-filled symbols). The star symbol accounts for the $D_{res}/2\pi$ value for a well-entangled melt of ≈140 kDa. Adapted with permission from Ref. [12] Copyright 2017 American Chemical Society.

As shown in Fig. 4.1.5,a linear dependence of D_{res} vs $(f-2)/f$, is observed in agreement with the predictions of the phantom model for the network elasticity..As observed, D_{res} approaches a value different from zero for $f = 2$. This is because the contribution of trapped entanglements to the network elasticity. A very good agreement is found for the value of D_{res}obtained by extrapolation to $f = 2$ ($D_{res}/2\pi \sim 82$ Hz) with the experimental value reported for well entangled PDMS polymer melts [58]. We can say that, NMR data predicts that these networks are well described by the phantom model for entangled strands. If to this fact we add the contribution of trapped entanglements and following the models by Lang and Sommer and Saalwächter et al. [41,59–61], we can express the residual dipolar coupling constant D_{res}^{df} for defect-free networks as

$$D_{res}^{df}\Big/2\pi = \frac{A}{M_c}\frac{(f-2)}{f} + T_e D^0\Big/2\pi \tag{4.6}$$

where M_c is the molecular weight between cross-links, $D^o/2\pi$ is the residual dipolar coupling associated with a well-entangled melt, T_e is the fraction of trapped entanglements, and the proportionality factor A depends on the polymer system The values obtained for $A = 2400$ Hz kg/mol an $T_e = 0.91$, by fitting the data of figure 4.3.4 are in good agreement with values obtained through rheology and theoretical predictions [12,39,62]. A very important result is that, NMR experiments confirm that the sources of elasticity for these networks are the elastically active chains, cross-link points, and trapped entanglements. Additionally, the linear behavior of D_{res} vs $(f-2)/f$ shows that the topology of the network does not affect the fraction of trapped entanglements.

The phantom model does not completely describe the dipolar couplings obtained for networks with defects as can see in Figure 4.3.4. We can observe that, dipolar interactions decrease with the presence of pendant material. If the time scale of NMR $\tau_{NMR} \lesssim \tau_e$, where τ_e is the Rouse time between entanglements, pendant material contributes to D_{res} as elastic chains. Therefore there is a temperature dependence in the contribution of pendant chains to D_{res}. As temperature increases a smaller fraction of trapped entanglements contributes to D_{res}.

On the other hand, it is known that in the presence of a Θ solvent the plateau modulus G_0 of well-entangled polymer melts scales as $G_0 \propto \phi^{7/3}$, where ϕ is the polymer concentration in the solution [17,63]. We can assume that the relaxed fraction $1-\phi$ of pendant materials acts like a Θ to the network elasticity [32,33,36,37]. This fraction is obtained through time-domain NMR experiments [49], being ϕ the relative contribution of the solid-like contribution. A striking result is shown in Fig. 4.1.6. There $D_{res}$is plotted against $\frac{f-2}{fM_{nB2}}\phi^{7/3}$, the full data set shows a simple linear dependence, independently of the functionality, temperature of analysis, the content of defects, or molecular weight of pendant chains.

We have been able to build a consistent picture establishing the relation between molecular microstructure and macroscopic elasticity of networks. The data presented represent a consistent validity of the phantom model for polymer networks containing different types of defects.

4.2. Semicrystalline polymers high-resolution 1D and 2D experiments and relaxation times

Linear polymers such as poly(ethylenimine) (PEI), polyampholyte and polyelectrolyte polymers, and particularly their metal complexes, have many practical and industrial applications. For example, PEI has been used as nonviral gene delivery vehicles and their Cu(II) complexes can be applied to the removal of heavy metal ions and for the degradation of pollutants with high environmental impact. We have used the effect of the strong relaxation of Cu on the ^{13}C spectra to get inside in the structural properties of Cu complexes. Additionally, 2D WISE an HETCOR experiments provided valuable information on the heterogeneity of the samples.

4.2.1. Polyampholite and polyelectrolite polymers

Solid-state NMR is a powerful techniques to characterize the hydrogels and their Cu(II)-complexes. It can elucidate, in particular, the coordination role of carboxylic acid and heterocyclic azole groups (imidazole, triazole and pyrazole), in the copper ion coordination sphere. Also, changes in the structural network can be observed by a combination of thermal and NMR experiments. In this section we focus on results obtained from the NMR techniques performed in the loaded and unloaded hydrogels, by using ^{13}C CP-MAS spectra, proton and carbon relaxation times (observed through ^{13}C), and ^{1}H–^{13}C WISE experiments.

Hydrogels were synthesized with ethylene glycol diglycidyl ether

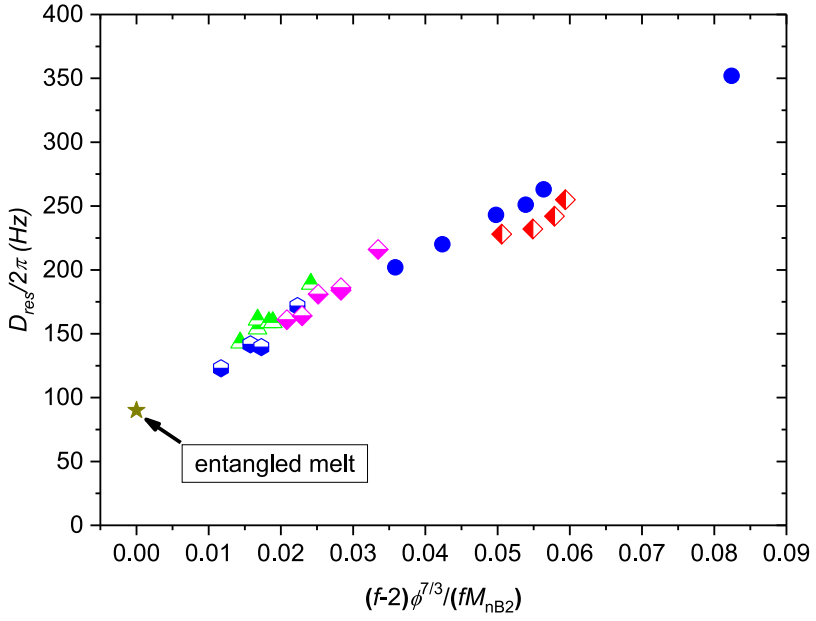

Fig. 4.1.6. D_{res} data vs experimental values for $(f-2)/(fM_{nB2})\ \phi^{7/3}$ for different sets of polymer networks (symbols: see details in Figure 4.3.5; star symbol corresponds to low molecular weight PDMS melt (≈ 30 kDa)). Adapted with permission from Ref. [12] Copyright 2017 American Chemical Society.

(EGDE), methacrylic acid (MAA) and/or nitrogen heterocycle monomers (IM = imidazole, 2MI = 2-methylimidazole, PYR = pyrazole, or TRZ = triazole). The abbreviations for the compounds with different amounts of copper concentrations are: "Xy", where "X" corresponds to the polymer matrix involved, Poly(EGDE-MAA)=*A*, Poly(EGDE-MAA-IM)=*B*, Poly(EGDE-2MI)=C, Poly(EGDE-MAA-TRZ)=*D*, Poly(EGDE-MAA-PYR)=*E*, and the subscript "y" corresponds to the mg of Cu(II) per gram of polymer. The molecular structures and synthesis route can be found in references [15,64,65].

The carbon CP-MAS spectra of the copper complexes of polymers A, B, C, D, and E, were determinant for the evaluation of the coordination role of the carboxylic acid in comparison with the azole rings in each case (imidazole, triazole, and pyrazole). Moreover, 2D ^{1}H–^{13}C wide line separation spectra (WISE), which provide the ^{1}H linewidth associated with the nearby carbons, were important to detect structural changes with complexation. Relaxation times in the rotating frame observed through carbon spectra were valuable to detect the effect of the copper coordination in certain sites. In all these samples, in addition to SSNMR, other solid-state techniques were used to complement the material characterization: Infrared, DSC and TG analysis, EPR, and X-ray diffraction, which supported the results. In this section, we focus on the information obtained from SSNMR.

One of our most important results in these copper complexes was obtained by analyzing the diminishing intensity of the carbon signal corresponding to the carboxylic group, C(1), about the copper concentration. This fact gave evidence of the important role of this carbon group in the coordination, in relation to the azole rings, in which carbon signals were practically unaltered in the copper complexes in comparison with the pure compound. The disappearance of this signal was probably due to the strong relaxation produced by the proximity between C(1) and the paramagnetic copper ion. This fact was in agreement with the FTIR results for each complex.

In particular, in the carbon spectrum of A_1 (without imidazole rings), the absence of carboxylic carbon in the carbon spectrum was evident. In the case of copper complexes of Poly(EGDE-MAA-IM)=*B*, it was possible to see that C(1) (and other carbons in MAA) were affected by the complexation, suffering a broadness for the small concentrations (B_8 and B_{26}) while being completely reduced for the highest concentrations (B_{48} and B_{63}).

In polymers poly(EGDE-MAA-TRZ) = D and poly(EGDE-MAA-PYR) = E, the changes in intensity occurred mainly in the intensity of C(1) in the ^{13}C CP-MAS spectra (see Fig. 4.2.1). Special care was taken in the selection of the contact times during the cross-polarization experiment since the relaxation times in the rotating frame were dramatically decreased as the copper ion adsorption increased. In the case of a polymer without MAA segment poly(EGDE-2MI) = C, and its copper complex C_{60}, the ^{13}C CP-MAS spectra were acquired with different contact times to observe changes in the signals, in a system that contains only imidazole groups. In this material, the number of available ligands was around 85%, whereas the remaining 15% was N1, N3-disubstituted. Reducing the contact time (from 600 to 1000 ms) the intensity of the imidazole signals of C_{60} was highly affected indicating that the copper ion produced a strong decrease in the relaxation times, especially for the carbons involved in the coordination [15].

As expected, all the proton and carbon relaxation times, $T_{H1\rho}$ and $T_{C1\rho}$, decreased with copper concentration for all the materials, see Table 4.2.1. The behavior was more related to the relaxation source provided by the copper complex than to the changes in molecular mobility that remain similar before and after the complexation. This is confirmed by the full width at half height (FWHH) obtained from the WISE Wide line Separation experiments. In general, the net tendency is a reduction in the polymeric mobility, induced by the cross-linking of the copper ion; this is associated with a reduction of the FWHH of the projection of the ^{1}H lines. In the case of triazole, there is a balance between this reduction and a polyelectrolyte effect associated with the increase in the positive domains.

Table 4.2.1
$T_{C1\rho}$ values together with the full width at half height (FWHH) from the WISE experiments, corresponding to the indicated carbon signals in different polymers. The relaxation time values were obtained by fitting an exponential decay function to the experimental data. The uncertainty in all FWHH values was less than 2 kHz and for the relaxation times, the relative errors are within 5%.

Polymer	Carbon signal	$T_{C1\rho}$ (ms)	FWHH (kHz)
B	**C(3)**	**2.0**	**59**
B_{63}	**C(3)**	**1.1**	**46**
C	**C(3)**	**1.9**	**57**
C_{60}	**C(3)**	**1.4**	**51**
D	**C(3)**	**2.4**	**64**
D_{40}	**C(3)**	**1.2**	**51**
E	**C(3)**	**2.9**	**50**
E_{19}	**C(3)**	**2.5**	**59**
PEI 87 kDa lyophilized	**44.5/42.9 ppm**	**—**	**43/71**
PEI 87 kDa crystallized	**42.9 ppm**	**—**	**80**
Cu(II)-PEI 87 kDa	**44.5 ppm**	**—**	**75**

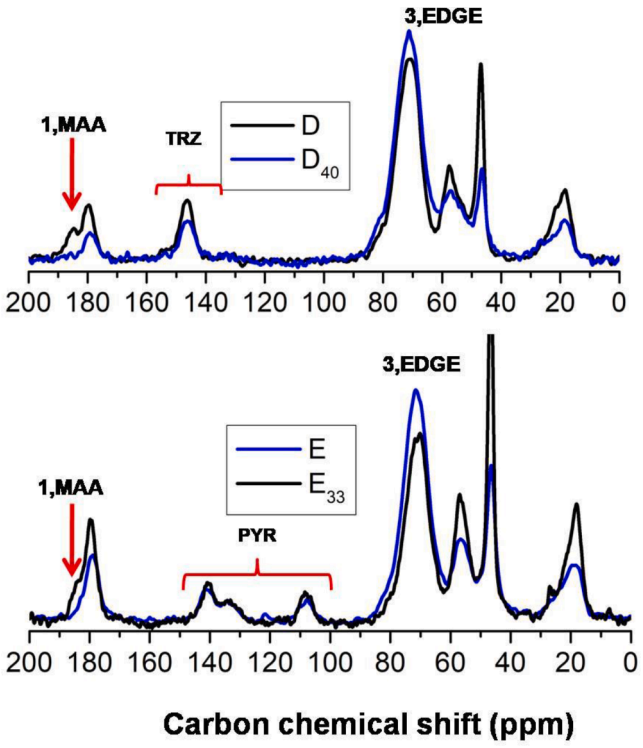

Fig. 4.2.1. ^{13}C CP-MAS spectra of *D*=Poly(EGDE-MAA-TRZ) and *E*=Poly (EGDE-MAA-PYR), and the corresponding copper complexes, D_{40} and E_{30}, the maximum available copper concentration per gram of polymer. The contact time for D and E was 1.5 ms (spectra in black line), while for the copper complexes were 0.8 ms (spectra in blue line). Some signals have been marked: carboxylic carbon C(1) belonging to the methacrylic acid, signal C(3) corresponding to EDGE segment, and the group of signals corresponding to the azole groups. The red arrow points to the C(1) signal which is highly affected and disappears with the copper concentration. Adapted with permission from Ref. [15] Copyright 2013 Elsevier.

4.2.2. Heterogeneous character of PEI polymers and edition spectra

By performing 1D and 2D ssNMR spectroscopy techniques, we were able to describe the structural and dynamic homogeneity of three synthetic variants of linear poly(ethylenimine hydrochloride), called PEI, in their crystallized or lyophilized states. Structural changes after the uptake of Cu(II) ion by these polymeric matrices were explored, given their importance in environmental applications [16].

Linear poly(ethylenimine hydrochloride) (PEI·HCl) polymers, called PEI, with different molecular weights of 22, 87, and 217 kDa (n = 505,2020,5050 respectively, see molecular structure in Figs. 4.2.2 and 4.2.3) were synthesized with two mechanisms that produced "lyophilized" and "crystallized" PEI samples [14]. These samples were complexed with copper to form the Cu(II)−PEI complexes. The only group of carbons present in the sample is (-CH2-), thus any multiplicity of signals in the carbon spectra correspond to different structural domains.

It is interesting to analyze the heterogeneity of PEI samples and particularly the effect of Cu complexation on lyophilized samples. Different types of CP-MAS sequences were applied, such as delayed CP-MAS, spin lock SL/CP-MAS and dipolar filter DF/CP-MAS. We will describe the results obtained on PEI 22 KDa samples, details for other samples can be found in the reference [14].

Fig. 4.2.2 shows various carbon spectra for the PEI 22 kDa sample. In particular, the standard CP and delayed CP for the crystallized sample, and the corresponding experiments for the copper complex. Note that the standard CP was acquired with a contact time of 1.5 ms while the delayed CP was acquired using 0.2 ms to avoid spin diffusion effects, and less intensity was observed. The standard CP for the PEI 22 kDa displays a simple resonance at 42.6 ppm with an additional shoulder. When applying a delay, the signal of the shoulder at 44.5 ppm increases, being appreciable for a t_d = 13 μs (red spectrum in figure 4.4.2). This gives evidence of a co-existence of domains of different mobility in this PEI polymer. In the case of copper complexes, the standard CP reveals a single resonance at 44.2 ppm and the same for the delayed CP (with diminished intensity because of the contact time and the delay), observing that the copper complex is homogeneous. These facts, and the changes observed in the XRPD spectra, indicate that some rearrangement took place after the uptake of Cu and SO4 2− ions. The absence of a second signal could have originated in the presence of copper, which induces the rapid relaxation of the nucleus in the proximity of the paramagnetic ion.

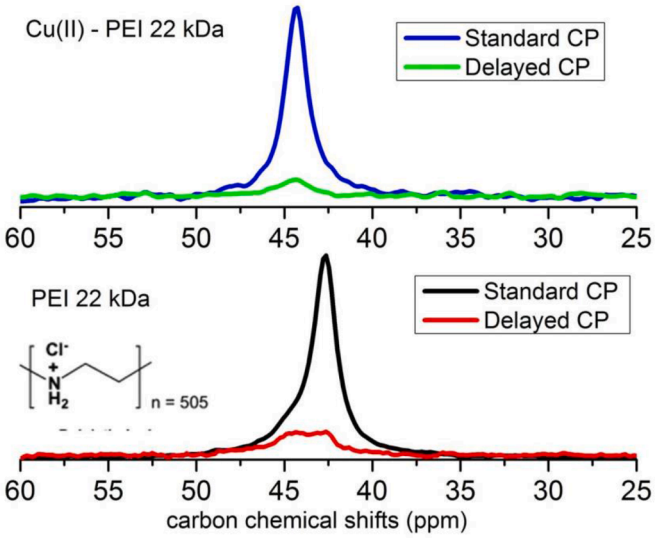

Fig. 4.2.2. ^{13}C CP-MAS spectra (standard and delayed) of PEI 22 kDa and its copper complex. See the molecular structure in the bottom figure. Note that standard CP is acquired with a contact time of 1.5 ms, while the delayed CP with a delay of 13 μs is acquired with 0.2 ms and thus it shows less intensity. Adapted with permission from Ref. [14], American Chemical Society.

On the other hand, the ^{13}C DF/CP-MAS technique, sensitive to mobile components, and ^{13}C SL/CP-MAS experiment, effective to select ^{13}C magnetization of rigid domains, were also performed for all the samples. The ^{13}C DF and SL/CP-MAS spectra were acquired and compared with the standard CP-MAS for the crystallized and lyophilized samples of PEI. In the case of the lyophilized sample, the ^{13}C SL/CP-MAS spectrum exhibited a signal at 42.9 ppm more intensely. Instead, the DF spectrum in the same sample, showed that the signal at 42.9 ppm was dramatically affected, while the signal at 44.5 ppm was practically unaltered. These results confirmed that resonances at 44.5 ppm and 42.9 ppm arise from the magnetization of environments in the amorphous and crystalline regions, respectively.

4.2.3. 2D experiments of PEI polymers

Fig. 4.2.3 shows the 2D ^{1}H–^{13}C WISE spectrum for PEI 87 kDa without copper (red projections and contour level) and after complexation (black contour level). The average line width of the ^{1}H resonance line projections in WISE experiments is a measure of the ^{1}H–^{1}H dipolar interactions. In the non-complexed sample, the ^{1}H projection and FWHH reinforce the idea that PEI samples are not homogenous. The smaller FWHH corresponds to the carbon signal at 44.5 ppm, whereas the higher FWHH corresponds to the carbon resonance at 42.9 ppm in all the samples, confirming the assignment made for each signal from the carbon edition. In the Cu complexes, the line width of the ^{1}H projection of the carbon at 44.5 ppm, the only signal that remains, showed a significant increase in comparison with the same projection in the sample without copper. This observation indicated that mobility was reduced with the coordination of the Cu ions. As an example, see Table 4.2.1 for PEI 87 kDa, the FWHH were 43 / 71 kHz for the signals at 44.5 / 42.9 ppm in the lyophilized sample, while in the crystallized this measure was 80 kHz and in the copper complex it took the uniform value of 75 kHz. The same behavior was observed for other molecular weight samples.

The 2D ^{1}H–^{13}C HETCOR spectra allowed correlating the different ^{13}C nuclei with the protons that were directly linked or nearby. In both samples of PEI 87 KDa, the methylene carbons (45–42 ppm) correlated with their directly bounded protons (~ 3 ppm) as well as with the non-bounded protons of the amino groups (~ 9 ppm). Carbon at 42.9 ppm correlated to protons with higher ^{1}H chemical shifts, than the more mobile components, which correlated with the 44.5 ppm carbon signal. This indicates that the polymer chains were in different physical environments, that is regions with a high degree of order (crystalline) or disorder (amorphous), in concordance with the information obtained from the edited ^{13}C CP-MAS spectra and XRPD experiments. For the Cu complexes, the signals observed may arise from the non-coordinated segments since Cu ions induce a strong source of relaxation. However, the changes in the 2D spectrum with PEI and Cu ions showed a homogeneous character of the complexed samples, with a shift in carbon and a non-appreciable shift in the correlated protons. In general, the observations corresponding to the 2D experiments performed in the PEI 27 kDa and 217 kDa samples are coincident with the behavior observed for PEI 87 kDa.

5. Conclusion

In this review, we have shown several applications of SSNMR for the characterization of polymeric compounds. We have presented various works carried out at the NMR group of the Facultad de Matemática, Astronomía, Física y Computación of Universidad Nacional de Córdoba in Argentina.

Our results show that time-domain NMR applied to dry polymer networks is a valuable alternative for structure determination and complements the indirect swelling and rheological methods traditionally used in polymer science. Using the DQ NMR technique, minor relative variations of average molecular weight between cross-linking

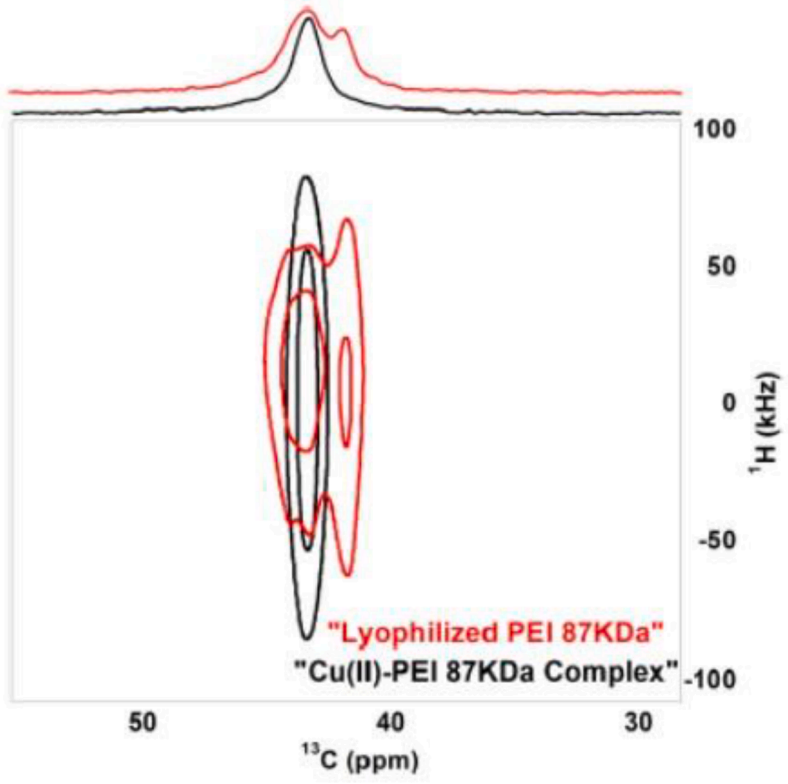

Fig. 4.2.3. ^{1}H–^{13}C WISE experiment of PEI 87 kDa (red) and its copper complex (black) . The direct and indirect projections display the carbon and proton spectra, respectively. Note that after complexation only the contribution from the signal at 44.5 ppm remains and a change of structure is observed from the wider proton projection associated. Reproduced with permission from Ref. [14], Copyright 2015 American Chemical Society.

points, pendant chain molecular weight, and pendant chain concentration can be analyzed. Even for such low concentrations of defects, DQ NMR appears to be a very sensitive parameter to probe variations of the molecular weight of elastically active chains as well as variations of both the concentration and the molecular weight of the pendant chains. We also have shown that the slow dynamics of PDMS network defects can be directly monitored by NMR spin relaxation of protons as a function of temperature. Application of the time−temperature superposition principle to transverse relaxation NMR parameters allows an accurate determination of the contribution of different types of defects to the relaxation processes. As high-temperature experiments ensure complete relaxation of the guest linear chains, accurate quantification of the content of elastic and pendant chains within the network is possible. On the other hand, we have proved that T_2 relaxation and DQ NMR experiments can provide a fast and highly effective microscopic technique to test different theories for network elasticity and quantify the key network parameters that control both, elastic and dissipative properties.

Polyelectrolytes and their complexes have been used in many applications as catalytic reactions such as hydrolysis of organophosphates and unimolecular decarboxylation. Polyampholyte–metal complexes have been proven to exhibit catalase-like activity in hydrogen peroxide decomposition, selective oxidation of organic substrates with hydrogen peroxide, and hydrogenation of ketones among other examples. Due to its biocompatibility, PEI and its complexes have been used in biotechnology as a nonviral vector to carry out gene transfection processes. Most of these polymers present heterogeneity in their structures, i.e. crystalline and amorphous character or different mobilities of the constitutive segments. In our works, we proved that SSNMR is a valuable tool to study the dynamics and homogeneity through edited ^{13}C CP-MAS spectra allowing demonstration of the heterogeneity in crystallized and lyophilized samples, associated with the presence of crystalline and amorphous domains. In addition, the results of 2D ^{1}H−^{13}C WISE and HETCOR experiments showed coexisting polymeric regions with different chemical environments Fig. 3.1.1.

Declaration of Competing Interest

The authors declare that they have no known competing financial interests or personal relationships that could have appeared to influence the work reported in this paper.

Data availability

Data will be made available on request.

Acknowledgments

We thank the financial support from Consejo Nacional de Investigaciones Científicas y Técnias (CONICET): 11220200100870CO, Secretaría de Ciencia y Tecnología (SeCyT) Universidad Nacional de Córdoba: 33620180100221CB, and Agencia Nacional para la Promoción de la Ciencia y la Técnica (ANPCYT): PICT 2019–02802.

References

[1] H. Staudinger, J. Fritschi, Über Isopren und Kautschuk. 5. Mitteilung. Über die Hydrierung des Kautschuks und über seine Konstitution, Helv. Chim. Acta 5 (1922) 785–806, https://doi.org/10.1002/hlca.19220050517.
[2] M.A. Voda, D.E. Demco, J. Perlo, R.A. Orza, B. Blümich, Multispin moments edited by multiple-quantum NMR: application to elastomers, J. Magn. Reson. 172 (2005) 98–109, https://doi.org/10.1016/j.jmr.2004.10.001.
[3] K. Saalwächter, Proton multiple-quantum NMR for the study of chain dynamics and structural constraints in polymeric soft materials, Prog. Nucl. Magn. Reson. Spectrosc. 51 (2007) 1–35, https://doi.org/10.1016/j.pnmrs.2007.01.001.
[4] K. Saalwächter, P. Ziegler, O. Spyckerelle, B. Haidar, A. Vidal, J.U. Sommer, 1H multiple-quantum nuclear magnetic resonance investigations of molecular order distributions in poly(dimethylsiloxane) networks: evidence for a linear mixing law

in bimodal systems, J. Chem. Phys. 119 (2003) 3468–3482, https://doi.org/10.1063/1.1589000.
[5] M. Wang, M. Bertmer, D.E. Demco, B. Blu, Segmental and Local Chain Mobilities in Elastomers by 13 C-1 H Residual Heteronuclear Dipolar Couplings, (2004). 10.1021/jp048392.
[6] T. Dollase, R. Graf, A. Heuer, H.W. Spiess, Local order and chain dynamics in molten polymer blocks revealed by proton double-quantum NMR, Macromolecules 34 (2001) 298–309, https://doi.org/10.1021/ma0013915.
[7] A. Lozovoi, C. Mattea, A. Herrmann, E.A. Rössler, S. Stapf, N. Fatkullin, A. Lozovoi, C. Mattea, A. Herrmann, E.A. Rössler, S. Stapf, N. Fatkullin, Communication : proton NMR dipolar-correlation effect as a method for investigating segmental diffusion in polymer melts, 241101 (2016). 10.1063/1.4954664.
[8] N. Fatkullin, A. Gubaidullin, C. Mattea, S. Stapf, On the theory of the proton free induction decay and Hahn echo in polymer systems: the role of intermolecular magnetic dipole-dipole interactions and the modified Anderson-Weiss approximation, J. Chem. Phys. (2012) 137, https://doi.org/10.1063/1.4769977.
[9] P. Sotta, C. Fu, D.E. Demco, B. Blu, H.W. Spiess, Effect of Residual Dipolar Interactions on the NMR Relaxation in Cross-Linked Elastomers, 1996.
[10] K. Schmidt-Rohr, H.W. Spiess, Multidimensional Solid-State NMR and Polymers, Academic Press, San Diego, CA, 1996.
[11] R. Graf, A. Heuer, H.W. Spiess, Chain-Order Effects in Polymer Melts Probed by 1H Double-Quantum NMR Spectroscopy, Phys. Rev. Lett. 80 (1998) 5738–5741, https://doi.org/10.1103/PhysRevLett.80.5738.
[12] F. Campise, D.C. Agudelo, R.H. Acosta, M.A. Villar, E.M. Vallés, G.A. Monti, D. A. Vega, Contribution of Entanglements to Polymer Network Elasticity, Macromolecules (2017) 50, https://doi.org/10.1021/acs.macromol.6b02784.
[13] R.H. Acosta, G.A. Monti, M.A. Villar, E.M. Vallés, D.A. Vega, Transiently trapped entanglements in model polymer networks, Macromolecules (2009) 42, https://doi.org/10.1021/ma8025546.
[14] J. Manuel Lázaro-Martínez, E. Rodríguez-Castellón, D. Vega, G. Alberto Monti, A. Karina Chattah, Solid-state Studies of the Crystalline/Amorphous Character in Linear Poly(ethylenimine hydrochloride) (PEI·HCl) Polymers and Their Copper Complexes, Macromolecules 48 (2015) 1115–1125, https://doi.org/10.1021/ma5023082.
[15] J.M. Lázaro-Martínez, G.A. Monti, A.K. Chattah, Insights into the coordination sphere of copper ion in polymers containing carboxylic acid and azole groups, Polymer (Guildf) 54 (2013) 5214–5221, https://doi.org/10.1016/J.POLYMER.2013.07.036.
[16] J.M. Lázaro Martínez, A.K. Chattah, G.A. Monti, M.F. Leal Denis, G.Y. Buldain, V. Campo Dall' Orto, New copper(II) complexes of polyampholyte and polyelectrolyte polymers: solid-state NMR, FTIR, XRPD and thermal analyses, Polymer (Guildf) 49 (2008) 5482–5489, https://doi.org/10.1016/J.POLYMER.2008.10.011.
[17] M. Rubinstein, R.H. Colby, Polymer Physics, oxford university press, 2003.
[18] G.B. McKenna, R.J. Gaylord, Relaxation of crosslinked networks: theoretical models and apparent power law behaviour, Polymer (Guildf) 29 (1988) 2027–2032, https://doi.org/10.1016/0032-3861(88)90176-0.
[19] M.A. Villar, M.A. Bibbó, E.M. Vallés, Influence of Pendant Chains on Mechanical Properties of Model Poly(dimethylsiloxane) Networks. 1. Analysis of the Molecular Structure of the Network, Macromolecules 29 (1996) 4072–4080, https://doi.org/10.1021/ma9506593.
[20] M.A. Villar, E.M. Vallés, Influence of Pendant Chains on Mechanical Properties of Model Poly(dimethylsiloxane) Networks. 2. Viscoelastic Properties, Macromolecules 29 (1996) 4081–4089, https://doi.org/10.1021/ma9506602.
[21] H. Watanabe, Viscoelasticity and dynamics of entangled polymers, Prog. Polym. Sci. 24 (1999) 1253–1403, https://doi.org/10.1016/S0079-6700(99)00029-5.
[22] P.J. Flory, Principles of Polymer Chemistry, Cornell University Press, New York, 1953.
[23] E.M. Valles, C.W. Macosko, The Effect of Network Structure in the Equation of Rubber Elasticity, Rubber Chemistry and Technology. 49 (1976) 1232–1237. 10.5254/1.3535010.
[24] P. Rempp, J. Herz, G. Hild, C. Picot, Tailor-made networks: synthesis and properties, Pure Appl. Chem. 43 (1975) 77–96, https://doi.org/10.1351/pac197543010077.
[25] L.R.G. Treloar, The Physics of Rubber Elasticity, Oxford Classic Texts in the Physical Sciences, 3rd ed., Oxford University Press, Oxford, 1975.
[26] J.J. Hermans, Deformation and swelling of polymer networks containing comparatively long chains, Trans. Faraday Soc. 43 (1947) 591, https://doi.org/10.1039/tf9474300591.
[27] F.T. Wall, P.J. Flory, Statistical Thermodynamics of Rubber Elasticity, J. Chem. Phys. 19 (1951) 1435–1439, https://doi.org/10.1063/1.1748098.
[28] H.M. James, E. Guth, Theory of the Increase in Rigidity of Rubber during Cure, J. Chem. Phys. 15 (1947) 669–683, https://doi.org/10.1063/1.1746626.
[29] H.M. James, E. Guth, Theory of the Elastic Properties of Rubber, J. Chem. Phys. 11 (1943) 455–481, https://doi.org/10.1063/1.1723785.
[30] D.A. Vega, M.A. Villar, E.M. Vallès, C.A. Steren, G.A. Monti, Comparison of mean-field theory and^{1}h nmr transversal relaxation of poly(dimethylsiloxane) networks, Macromolecules 34 (2001).
[31] G. Simon, K. Baumann, W. Gronski, Mc determination and molecular dynamics in crosslinked 1,4-cis-polybutadiene: a comparison of transversal proton and deuterium NMR relaxation, Macromolecules 25 (1992) 3624–3628, https://doi.org/10.1021/ma00040a003.
[32] S.T. Milner, T.C.B. McLeish, Parameter-Free Theory for Stress Relaxation in Star Polymer Melts, Macromolecules 30 (1997) 2159–2166, https://doi.org/10.1021/ma961559f.
[33] D.A. Vega, L.R. Gómez, L.E. Roth, J.A. Ressia, M.A. Villar, E.M. Vallés, Arm Retraction Potential of Branched Polymers in the Absence of Dynamic Dilution, Phys. Rev. Lett. 95 (2005), 166002, https://doi.org/10.1103/PhysRevLett.95.166002.
[34] D.S. Pearson, E. Helfand, Viscoelastic properties of star-shaped polymers, Macromolecules 17 (1984) 888–895, https://doi.org/10.1021/ma00134a060.
[35] S. Shanbhag, R.G. Larson, Chain Retraction Potential in a Fixed Entanglement Network, Phys. Rev. Lett. 94 (2005), 076001, https://doi.org/10.1103/PhysRevLett.94.076001.
[36] T.C.B. McLeish, Tube theory of entangled polymer dynamics, Adv. Phys. 51 (2002) 1379–1527, https://doi.org/10.1080/00018730210153216.
[37] S.T. Milner, T.C.B. McLeish, Reptation and Contour-Length Fluctuations in Melts of Linear Polymers, Phys. Rev. Lett. 81 (1998) 725–728, https://doi.org/10.1103/PhysRevLett.81.725.
[38] F. Campise, Influencia De Los defectos, Entrelazamientos y Parámetros Estructurales En Las Propiedades Viscoláskticas Poliméricas modelo, Doctoral, Universidad Nacional de Cordoba, 2017.
[39] K. Saalwächter, M. Klüppel, H. Luo, H. Schneider, Chain order in filled SBR elastomers: a proton multiple-quantum NMR study, Appl. Magn. Reson. 27 (2004) 401–417, https://doi.org/10.1007/BF03166740.
[40] K. Saalwächter, P. Ziegler, O. Spyckerelle, B. Haidar, A. Vidal, J.-.U. Sommer, 1H multiple-quantum nuclear magnetic resonance investigations of molecular order distributions in poly(dimethylsiloxane) networks: evidence for a linear mixing law in bimodal systems, J. Chem. Phys. 119 (2003) 3468–3482, https://doi.org/10.1063/1.1589000.
[41] K. Saalwächter, B. Herrero, M.A. López-Manchado, Chain Order and Cross-Link Density of Elastomers As Investigated by Proton Multiple-Quantum NMR, Macromolecules 38 (2005) 9650–9660, https://doi.org/10.1021/ma051238g.
[42] R. Stepto, Polymer Networks. Principles of Hteir formation, Structure and Properties, Chaoman and Hall, Bristol, 1997.
[43] L.E. Roth, D.A. Vega, E.M. Vallés, M.A. Villar, Viscoelastic properties of networks with low concentration of pendant chains, Polymer (Guildf) 45 (2004) 5923–5931, https://doi.org/10.1016/j.polymer.2004.06.043.
[44] D.R. Miller, C.W. Macosko, A New Derivation of Post Gel Properties of Network Polymers, Macromolecules 9 (1976) 206–211, https://doi.org/10.1021/ma60050a004.
[45] D.R. Miller, E.M. Valles, C.W. Macosko, Calculation of molecular parameters for stepwise polyfunctional polymerization, Polym. Eng. Sci. 19 (1979) 272–283, https://doi.org/10.1002/pen.760190409.
[46] R.H. Acosta, D.A. Vega, M.A. Villar, G.A. Monti, E.M. Vallés, Double quantum NMR applied to polymer networks with low concentration of pendant chains, Macromolecules (2006) 39, https://doi.org/10.1021/ma060011y.
[47] J.P. Cohen-Addad, Effect of the anisotropic chain motion in molten polymers: the solidlike contribution of the nonzero average dipolar coupling to NMR signals. Theoretical description, J. Chem. Phys. 60 (1974) 2440–2453, https://doi.org/10.1063/1.1681380.
[48] P. Sotta, C. Fülber, D.E. Demco, B. Blümich, H.W. Spiess, Effect of Residual Dipolar Interactions on the NMR Relaxation in Cross-Linked Elastomers, Macromolecules 29 (1996) 6222–6230, https://doi.org/10.1021/ma960141e.
[49] F. Campise, L.E. Roth, R.H. Acosta, M.A. Villar, E.M. Vallés, G.A. Monti, D.A. Vega, Contribution of Linear Guest and Structural Pendant Chains to Relaxational Dynamics in Model Polymer Networks Probed by Time-Domain ^{1}H NMR, Macromolecules (2016) 49, https://doi.org/10.1021/acs.macromol.5b01806.
[50] E.M. Valles, C.W. Macosko, Properties of Networks Formed by End Linking of Poly (dimethylsiloxane), Macromolecules 12 (1979) 673–679, https://doi.org/10.1021/ma60070a025.
[51] M. Gottlieb, C.W. Macosko, G.S. Benjamin, K.O. Meyers, E.W. Merrill, Equilibrium modulus of model poly(dimethylsiloxane) networks, Macromolecules 14 (1981) 1039–1046, https://doi.org/10.1021/ma50005a028.
[52] M. Zhong, R. Wang, K. Kawamoto, B.D. Olsen, J.A. Johnson, Quantifying the impact of molecular defects on polymer network elasticity, Science 353 (2016) (1979) 1264–1268, https://doi.org/10.1126/science.aag0184.
[53] R.C. Ball, M. Doi, S.F. Edwards, M. Warner, Elasticity of entangled networks, Polymer (Guildf) 22 (1981) 1010–1018, https://doi.org/10.1016/0032-3861(81)90284-6.
[54] S.F. Edwards, T.A. Vilgis, The tube model theory of rubber elasticity, Rep. Progr. Phys. 51 (1988) 243–297, https://doi.org/10.1088/0034-4885/51/2/003.
[55] B. Erman, J.E. Mark, Rubber-Like Elasticity, Annu. Rev. Phys. Chem. 40 (1989) 351–374, https://doi.org/10.1146/annurev.pc.40.100189.002031.
[56] G. Heinrich, E. Straube, G. Helmis, Rubber elasticity of polymer networks: theories, in: 1988: pp. 33–87. 10.1007/BFb0024050.
[57] T.A. Vilgis, B. Erman, Comparison of the constrained junction and the slip-link models of rubber elasticity, Macromolecules 26 (1993) 6657–6659, https://doi.org/10.1021/ma00076a055.
[58] L.E. Roth, E.M. Vallés, M.A. Villar, Bulk hydrosilylation reaction of poly (dimethylsiloxane) chains catalyzed by a platinum salt: effect of the initial concentration of reactive groups on the final extent of reaction, J. Polym. Sci. A Polym. Chem. 41 (2003) 1099–1106, https://doi.org/10.1002/pola.10649.
[59] W. Chassé, M. Lang, J.-.U. Sommer, K. Saalwächter, Cross-Link Density Estimation of PDMS Networks with Precise Consideration of Networks Defects, Macromolecules 45 (2012) 899–912, https://doi.org/10.1021/ma202030z.
[60] M. Lang, J.-.U. Sommer, Analysis of Entanglement Length and Segmental Order Parameter in Polymer Networks, Phys. Rev. Lett. 104 (2010), 177801, https://doi.org/10.1103/PhysRevLett.104.177801.
[61] I.H. Syed, P. Stratmann, G. Hempel, M. Klüppel, K. Saalwächter, Entanglements, Defects, and Inhomogeneities in Nitrile Butadiene Rubbers: macroscopic versus

Microscopic Properties, Macromolecules 49 (2016) 9004–9016, https://doi.org/10.1021/acs.macromol.6b01802.
[62] C. Tsenoglou, Rubber elasticity of cross-linked networks with trapped entanglements and dangling chains, Macromolecules 22 (1989) 284–289, https://doi.org/10.1021/ma00191a052.
[63] L.E. Roth, D.C. Agudelo, J.A. Ressia, L.R. Gómez, E.M. Vallés, M.A. Villar, D. A. Vega, Viscoelastic response of linear defects trapped in polymer networks, Eur. Polym. J. 64 (2015) 1–9, https://doi.org/10.1016/j.eurpolymj.2014.12.036.
[64] J.M. Lázaro Martínez, M.F. Leal Denis, V. Campo Dall'Orto, G.Y. Buldain, Synthesis, FTIR, solid-state NMR and SEM studies of novel polyampholytes or polyelectrolytes obtained from EGDE, MAA and imidazoles, Eur. Polym. J. 44 (2008) 392–407, https://doi.org/10.1016/j.eurpolymj.2007.11.022.
[65] J.M. Lázaro Martínez, A.K. Chattah, R.M. Torres Sánchez, G.Y. Buldain, V. Campo Dall' Orto, Synthesis and characterization of novel polyampholyte and polyelectrolyte polymers containing imidazole, triazole or pyrazole, Polymer (Guildf). 53 (2012) 1288–1297. 10.1016/j.polymer.2012.01.031.